

# A Wavelet Exploration of the Q0957+561 A,B Brightness Record

R. Schild

Center for Astrophysics, 60 Garden Street, Cambridge MA 02138

rschild@cfa.harvard.edu

Received \_\_\_\_\_; accepted \_\_\_\_\_

## ABSTRACT

We analyze the Q0957+561 A,B brightness record with 3 types of wavelets to define properties that are independent of the nature of the analyzing wavelet. The wavelet analysis picks out features having arbitrary shape, and localizes them in time and fits amplitudes.

We find that independently of the analyzing wavelet, the mean wavelet amplitude is zero, meaning that there are as many positive as negative brightness spikes. For all wavelet durations the fitted amplitudes are equal in the A and B images, except that image B may have larger amplitude brightness fluctuations for the longest duration 64-day features. Independently of the wavelet family fitted or of the kind of statistical measure of wavelet amplitude, the fitted amplitudes seem to increase as a linear function of the wavelet duration, with the mean absolute deviation about a factor of 10 greater for 64-day wavelets than for 2-day wavelets. The underlying physical process producing the brightness fluctuations is found to have more power in long duration wavelets than in short duration wavelets than a process dominated by white noise. Thus it is established that the rapid brightness fluctuations observed in the Q0957 images A and B are not the result of observational noise.

*Subject headings:* cosmology:observations–dark matter: microlensing–quasar–dark matter: wavelets–quasar brightness

## 1. Introduction: Why Wavelet Analysis?

The Q0957+561 brightness record provides a unique data stream for the exploration of quasar brightness fluctuations modified by microlensing. The data have been consistently reported from CCD observations since the object’s discovery in 1979, and by now data for 1200 nights of observation are available, with a nightly average brightness reported by Schild and Thomson (1996) and earlier references. Although the original 1986 Schild and Cholfin time delay has long been controversial, it is now confirmed by radio and optical data (Haarsma et al 1997). The optical CCD data have recently been analyzed by Pelt et al (1996, 1998), Pijpers and Wanders (1997), Thomson and Schild (1997), and Goicoechea et al (1998) for time delay between arrival of the two quasar images. With the time delay now satisfactorily determined and the cosmological implications for the determination of the Hubble Constant amply discussed by Kundic et al (1997), it is time to consider other results mined from the Q0957 brightness record.

The most obvious feature of the Q0957 data record is the unexpected rapid brightness fluctuations of low amplitude found. It has long been known that these features cannot be intrinsic to the quasar, because if they were the time delay would have been easy to determine. Many authors have published cross-correlation or equivalent calculations for the determination of time delay, and the Full Width at Half Maximum or some equivalent measure of the width of the autocorrelation peak always is found to be of order 100 days, as was found even in the first successful autocorrelation calculation of Schild and Cholfin (1986). This probably means that the high frequency part of the brightness record does not originate in intrinsic quasar brightness fluctuations. A more direct demonstration of this is found in the calculations of Pelt et al (1996, Figs. 10 and 11), where the brightness fluctuation time series was filtered and separated into high-frequency and low-frequency components. These authors then demonstrated that the high-frequency part of the

brightness record does not show the 415 day time delay; the low frequency part does.

Because the high frequency component of the quasar’s brightness record does not display the time delay, it seems likely it originates in microlensing, although the exact mechanism is unclear. Schild(1996) has discussed the probable origin in a population of planetary mass objects in the lens galaxy, but has noted that for such an explanation to be viable the quasar source must have structure on a scale comparable to the size of the Einstein ring for a  $10^{-6}M_{\odot}$  microlens in the lens galaxy. Gould and Miralda-Escude (1997) concur with the general findings of Schild regarding the microlensing origin, and suggest that some quasar source structure may be in motion to modify the relevant time scales. Because no detailed model calculation of the rapid microlensing exists, it would have to be said that the nature of the microlensing is as yet not understood. Schild (1996) considers the possibility that the fluctuations originate in part in mass particles in the Halo of our Galaxy, or in the quasar host galaxy, and a microlensing calculation with two lens screens may be required. Given that Schild (1996) and Gould and Miralde-Escudo (1997) all attribute the rapid brightness fluctuations to microlensing, for the remainder of this report we refer to them as microlensing.

Although questions remain about the accuracy of the Mount Hopkins data which define the microlensing, in the one situation where direct comparison with other observatories is possible, the data and the rapid microlensing are confirmed (Gibson and Schild 1999). A more comprehensive discussion of the microlensing has been given by Schild (1996), who finds that the microlensing is seen as a continuous pattern of brightness peaks having cusp-shaped profiles and amplitudes of several percent (see Schild 1996 Fig. 2). An excellent example of a microlensing event seen in the brightness record of the A image is given as Fig. 5 of Schild 1996. That profile shows a 90-day event well above the observational noise, together with a nearly continuous pattern of lower amplitude events which are

barely recognizable above the noise of the brightness detection. These weak features are admittedly poorly determined, because their amplitude is barely, or not even, above the noise level, shown as the grey zone in that illustration. However, even though an individual data point is in the grey noise zone, the data points form distinctive trends that indicate cusp-shaped profiles in a nearly continuous pattern. The situation is similar to Q2237, where it is generally considered that microlensing has been observed because even though the individual data points do not significantly prove microlensing, their overall trend is considered convincing (Corrigan 1991). And in the one case where the quasar has been amply observed by 3 observatories concurrently, a 30-day microlensing event was distinctly seen (Gibson and Schild 1999).

An inspection of the microlensing record of Fig. 2 in Schild (1996) seems to suggest that the strongest microlensing events have a peak amplitude of about 0.10 mag and duration of about 1/4 year. Their profiles seem to be more cusp-like than sinusoidal. Thus it would seem *ab initio* that they are better described by wavelets than by sines and cosines. Moreover, in the present writing we are not concerned about periodic effects in the cusp features, but rather just in the most elementary statistical description of the amount of power as a function of duration of the features. Because a wavelet analysis provides the mathematical tools to perform a multiscale correlation analysis with an analyzing function similar to the details of the observed and expected fluctuations, it provides an optimum methodology for our application.

The first wavelet analysis applied to the Q0957 system was reported by Hjorth et al(1992) for the determination of time delay. The conclusion of the application was that the time delay was not determined, but this report contains an excellent statement of the nature of wavelet analysis. This author also finds particularly useful the book Wavelets in Geophysics by Foufoula-Georgiou and Kumar (1994) for examples of applications in

physical science, with many references to more theoretical texts. Early developments of the wavelet theory were given by Mallat(1989), and the first application to problems in astronomy was by Slezak, Bijaoui, and Mars (1990); the first review of wavelet analysis in astronomy was given by Scargle (1997),

Although our discussion is oriented toward microlensing, we in fact analyze the separate A and B brightness records. While in principal microlensing should be studied by subtracting the time delay shifted B from the A component brightness record, to do so loses information about which image causes the fluctuations. We have previously noted that the quasar’s rapid brightness fluctuations on time scales up to 100 days seem to be dominated by microlensing and our purpose here is to demonstrate properties of rapid brightness fluctuations in the two image components.

## 2. The Data Set

Because our basic data sampling is once nightly, a Nyquist argument gives our basic wavelet resolution lower limit of 2 days, and this is the shortest duration wavelet we will fit to the data. Optimum fitting dictates that wavelets of increasing powers of two be subsequently fitted, so the wavelets are of duration 2, 4, 8, 16, 32, ... days. A major problem is that the data record has many missing nights, and to minimize this problem we investigate only the data subset of the last four observing seasons, when observations were attempted nightly during the 9-month observing season. As will be discussed below, corrections for missing data will be derived and applied to the results. The observing season for Q0957 starts on Oct 1 and ends June 30 the following year. Data for the 1992-93 and 1993-94 have been published by Schild and Thomson (1996) and data for the two following seasons are available in tabular form from the author’s homepage <http://cfa-www.harvard.edu/rschild/> and have already been analyzed by some authors (Goicoechea et al 1998).

Because the data are incomplete they will need to be interpolated for the present program. We have of course experimented with several methods of interpolation over the years, but simple linear interpolation seems best for the present effort. Linear interpolation cannot increase wavelet power at any frequency, whereas other schemes might. And with linear interpolation, corrections for missing data are conceptually and computationally simplest.

### 3. Analysis

As yet no particular wavelet or wavelet family has been shown to be optimal for microlensing investigations, and we will try three examples known to have different properties to see if any significant differences are found. The wavelet literature is full of considerations of orthonormality of wavelets, which relates to optimum compression of signals or optimum signal reconstruction. We are more simply concerned with how effectively the various wavelet types fit our cusp-shaped data profiles, and our approach will be to try three different choices to see whether and how the results agree. However we are also anticipating future developments and will concentrate on wavelets with the most useful properties

Our first choice will be the Coiflet 2 (coif2) wavelet displayed in Fig 1a. It is a nearly symmetrical wavelet with a scaling function, also shown in Fig 1a. As with all wavelets, it has positive and negative components so its integral is unity; of course the positive spike predominates in the fitting process. The Coiflet wavelets are orthogonal, biorthogonal, and have compact support; they are useful for discrete wavelet transforms and for continuous wavelet transforms. They are generally regarded as compactly supported wavelets with the highest number of vanishing moments for both  $\phi$  and  $\psi$  for a given support width.

Our second two choices are asymmetrical and part of the orthonormal set of wavelets by Daubechies. As illustrated , the Daubechies 2 (Db2 Fig 1b) and Daubechies 3 (Db3, Fig 1c) wavelets are asymmetrical and have negative side-lobes of different character. Our purpose in including these two alternatives is to test whether the wavelet fits give results which are significantly dependent on the wavelet type. Like the Coiflets, the Daubechies wavelets are known as compactly supported wavelets with the largest number of vanishing moments for a given support width. They are orthogonal, biorthogonal, have compact support, and are useful for discrete and continuous wavelet transforms. Their associated scaling filters are minimum-phase filters.

Figure 2 shows the wavelet decomposition of the Q0957+561 A image for a `coif2` wavelet, and in Fig. 3 shows the decomposition for image B. In both figures, the signal analyzed  $s$  is shown in the upper left panel and is the brightness record for the most recent 4 years when the quasar observation was scheduled nightly. Data from multiple images obtained the same night were averaged together for a single nightly average. In all of the panels of Figs. 2-4, the amplitudes of the wavelet coefficients and the residuals, as well as the original signal, are expressed in magnitude units. The zero point for the dates of observation was JD 2448901. Figures 2 and 3 show the decomposition of the A and B brightness records into wavelets of duration 2-64 days, plus a residual signal `a6`, as explained in the Figure 2 caption. The power of this approach is that the six detail signals `d1...d6` now provide the basis for detailed estimation of numerous properties of the original signal, such as the power in negative *vs* positive wavelets and the amount of wavelet power as a function of wavelet duration. Such properties obviously relate to the physical process producing the brightness fluctuations, and our purpose is to provide a quantitative means of comparing observations to model simulations.

Before deriving a catalogue of wavelet properties and determining and applying



corrections for the incompleteness of the data set in subsequent sections, we will provide an additional illustration to display some interesting properties of the wavelet fits. The impatient or sophisticated reader may prefer to skip to the next section.

Figure 4 shows the lowest order wavelet decomposition of a subset of the A data record analyzed previously. The date zero point and scale are the same as in Fig 2, and the data and results may be recognized as basically a zoom of a portion of that illustration. The subset was chosen because of the extraordinary quiescence of the quasar to daily brightness fluctuations, even though fluctuations on a time scale of 4 days, shown in the d2 box, were normal. From this data subset we conclude that the Mt Hopkins data are capable of recording very quiescent data at some frequencies, even as the fluctuations were more normal at lower frequencies. This has implications about the accuracy of the data, since to record quiescence at high frequencies requires both that the source be quiescent and that the data be of high quality. Schild (1990) had previously noted the surprising quiescence of the A image in 1988-89, and we may now consider this quasar/microlensing property confirmed from observations in the 1995-96 season. As regards accuracy of the data, we have long considered that the largest uncertainty in our monitoring data is from correlated power between the two closely spaced (6 arcsec separation) images due to seeing effects, as discussed in Appendix 1 of Schild and Cholfín (1986). However this effect should have its characteristic signature; if seeing gets worse, the enlarged quasar images spill over into one another and both images are measured to be too bright (recall that the basic photometric procedure is to measure the total luminosity contained within a 6 arcsec diameter aperture with the aperture photometry of 5 standard stars lacking close companions). Thus deteriorated seeing always produces comparable photometric errors in both images, and always in the sense of excess brightness. Because poor seeing spells at Mt Hopkins are usually experienced on time scales of a single night or portion of a night, correlated errors due to seeing effects should be seen on single day time scales. We may

conclude from Fig. 4 that since only very low amplitude fluctuations are found most of the time, seeing effects evidently do not affect the Mt Hopkins data at the 0.005 mag level. Comparison of the A and B brightness records for the period, as shown in Figs 2 and 3, shows that the B component showed the usual brightness fluctuations during the period.

A possibly troubling point also evident from inspection of figures 2 and 3 is the appearance that linear interpolation has caused large wavelet power at the ends of the interpolation intervals. These features are seen around date 1140 in fig. 2 and 1160 in Fig. 3. But a closer inspection will show that these features are well embedded in real data, as confirmed by our expanded scale calculations (not shown here). We in fact find no problem at the ends of the interpolation intervals.

## 4. Results

### 4.1. The Mean Values

We are now in a position to use the wavelet decompositions of the two time series of brightness data to ask simple questions about the physical process. Inspection of the details coefficients d1...d6 in Figs. 2-4 suggests that about as many positive as negative wavelets have been fitted to the brightness record. In other words, there are about as many downward as upward brightness spikes. Is this apparent in the statistics?

Table 1 shows the mean values of the wavelet decompositions d1 - d6 for the three types of wavelets, and for each quasar image. For each level of decomposition d1...d6 we calculate the mean value of fitted wavelets, and the rms deviation of the mean. The quantity for which we compute the mean value is the the amplitude of wavelets fitted to the time series, and if there is any significant tendency for the physical process to produce more positive than negative wavelets for some wavelet scale, then the means for the decompositions d1-d6

should differ significantly from zero independent of the shape of the analyzing wavelet. We find that the tabulated rms deviations of the means are in general larger than the means so we conclude no significant departures of the means are found for any level of decomposition. A possible exception is that for the finest details at level d1 (2-day wavelets) a small trend toward negative means may be found, but since it is a low-significance conclusion and is not seen in any of the other decomposition levels d2-d6, we dismiss it for now as a probable fluke (since in 12 statistical tests you would expect one 3-sigma event). The visual impressions of the decompositions in Figs. 2 and 3 are that positive and negative brightness spikes are about equally large and numerous for all wavelet scales.

Equal positive and negative brightness spikes are of fundamental importance because most astrophysical processes at low surface optical depth generate asymmetrical brightness curves. We know of two processes causing equal positive and negative features: microlensing at surface optical depths near unity (Schneider, Ehlers, and Falco, 1991, p. 343.), and microlensing by a double screen of microlenses, so that a second screen can decrease or increase the magnification caused by the first screen. We accept that it remains to be conclusively demonstrated that the brightness fluctuations seen in the two quasar images are dominated by microlensing, but we have already presented arguments that they probably are.

We do find in Table 1 a small tendency for the image B means to be more negative than positive, but in all cases the mean value is smaller than its rms deviation, and we do not claim a significant result. Note that since the wavelets are being fitted to data in magnitudes, a small negative mean would indicate a small preponderance of spikes of brightness increase.

## 4.2. The Mean Absolute Deviation

Table 2 shows the mean absolute deviation of the wavelet coefficients as a function of wavelet duration for the three wavelet types. The table lists under the column labeling the detail level corresponding to Figs. 2-4 and the wavelet duration expressed in days, the observed wavelet coefficients expressed in magnitudes. Thus the upper left table entry .002284 means that the mean absolute amplitude of Coif2 wavelets of 2-day duration fitted to the data record is .002284 mag. Proceeding down an individual column of Table 2, we list the mean absolute deviations for the three wavelet types, then the mean value and the rms deviation of the three values contributing to the mean. Then we list the derived corrections for incomplete sampling which depend on the wavelet duration, and finally we list the value of the mean absolute deviation corrected for incomplete sampling.

Figure 5 shows the means as a function of wavelet duration. From these results we reach the important conclusion, seen to be independent of wavelet type and seen to apply to both image components; *the short-term quasar fluctuations increase in amplitude with increasing wavelet duration*. We shall see below that this conclusion is not modified by corrections for incompleteness of the data record. We also find no significant difference in microlensing power between the A and B quasar images, except possibly for the longest, 64-day, wavelets considered here.

## 4.3. Corrections to the Mean Absolute Deviation for Incompleteness

The data in Figure 5 need correction for the fact that brightness monitoring was not possible during the summer months when the source is too close to the sun, and during bad weather spells or when the CCD camera was unavailable for one reason or another. The corrections will depend upon the duration of the fitted wavelet. For example, for the 64-day

wavelets, data missing for days or weeks should not affect the fitted profiles, and we expect only a correction for the long summer break. Thus the brightness record should be about 3/4 complete, and we expect a correction factor of approximately 4/3. For the shortest, 2-day wavelets fitted, the correction factor is the reciprocal of the fractional number of dates of observation, since a missing day’s data means that the program interpolates across the two adjacent data points, and cannot determine the correct wavelet amplitude. Thus for 2-day wavelets, the correction is the reciprocal fraction of the number of observation dates in the observing record, which is 471/1358. For wavelets of intermediate duration, the missing data corrections are similarly computed from the number of missing half-duration intervals, and the corrections are listed in Table 2 in the rows marked *corr*.

The Mean Absolute Deviation results for the wavelet fits are listed in Table 2 in the rows marked *crtld* and are plotted in Figure 6, where the amplitudes are shown as ordinates for abscissas plotted as the wavelet duration. The error bars express rms deviation of a mean value for the three wavelet types, to give some sense of the dependence of the mean absolute deviation on wavelet choice. In this plot we find a striking result that *the amplitudes are simply proportional to wavelet duration*. There is some suggestion that for image B, an additional component may be present at the longest, 64-day wavelets. If  $T$  is the wavelet duration in days and  $W$  is the Mean Absolute Deviation listed in the *ctd* rows of Table 2, then  $W = .00101(T) + .0063$ . As noted above, image B may have a slightly higher value for wavelets 64 days and longer.

The characterization of the underlying process producing brightness fluctuations in Fig. 6 is easily seen to differ from white noise, for which the average wavelet coefficients would be equal for all wavelet durations. In the Q0957 data set observational errors were estimated based upon multiple observations each night. If these observational errors had been significantly underestimated, to the extent that the rapid brightness fluctuations

reported are dominated by Gaussian statistical errors, the resulting process would be described as white noise. For a white noise process, the mean wavelet amplitudes expressed as either a mean absolute deviation or as a root mean square would be equal at all wavelet scales, which means that the line connecting the observational means in figures 5 - 8 would be a horizontal straight line. Such a line cannot fit the data, and we conclude that observational errors do not dominate the observed pattern of brightness fluctuations on time scales investigated here.

#### 4.4. The rms Mean

As a means of testing the robustness of our approach and conclusions, we consider a second measure of amplitude of the fitted wavelets. In the previous discussion, a linear measure of amplitude of the fitted wavelengths was adopted with the mean absolute deviation; we now adopt a quadratic measure, the root mean square (rms) deviation. This is the familiar statistical estimator with the well known properties that all deviations from the mean are squared and therefore positive, and that the several strongest peaks contribute most to the rms measure. Our treatment proceeds analogously to that for the MAD measure, and the new analogues to Table 2 and Figs 5 and 6 are Table 3 and Figs 7 and 8.

Figure 7 shows the Table 3 data for the uncorrected wavelet amplitudes (not corrected for incomplete sampling). Compared to figure 5, we find a larger scatter for the amplitudes expressed as an rms, especially at 32 and 64 day wavelets, presumably because the rms averages are more sensitive to the several largest amplitude wavelets. This sensitivity probably also accounts for the large discrepancy at 64-days between the amplitudes for the different wavelet types on the B image data. Nevertheless as was found for the MAD amplitude measure, the B quasar image seems to have more wavelet amplitude than image

A for the longest-duration wavelets.

In correcting the rms data to be plotted as Fig. 8 a procedural change must be made appropriate to the rms statistic. The corrections for the number of missing data points must now be entered with a harmonic mean instead of a linear multiplier. With this modification the *crted* data in Table 3 and Fig. 8 are obtained.

The corrected rms wavelet amplitudes shown in Fig 8 show one potentially important feature found previously in Fig. 6; the amplitudes of the wavelets agree to within the errors for all but the longest wavelets, and for these 64 day wavelets the B quasar image has the greatest amplitude. Recall that the B image is seen closer to the lens galaxy G1’s image, so image B has an optical depth to microlensing a factor approximately 3.3 larger than image A.

A property also common to both measures of wavelet amplitude is the upturn from a linear fit that occurs for the shortest, 2-day wavelets. This feature suggests that some excess power at the shortest 1-day timescale in the data set has a significant contribution from observational errors. This property was discussed in 3, and is somewhat dependent on the accuracy of the corrections applied for data incompleteness. We expect to return to this point in a future report in which we will examine several 80-day data subsets which have more complete sampling on the daily time scale.

From a fit to our corrected Table 3 data, as shown in Fig. 8, we determine a best fitting mean relation  $W = .00133 * T + .0060$ , with variables as defined in Section 4.3. We find for the wavelet coefficients expressed as a root mean square as we found for mean absolute deviation that the underlying process differs from a white noise process, which produces equal rms coefficient amplitudes at all wavelet scales.

## 5. Summary and Conclusions

In our first wavelet decomposition of the Q0957 brightness record, we have adopted the viewpoint that the predominant fluctuations originate in microlensing, not in intrinsic quasar fluctuations. This follows as a conclusion from the Pelt et al (1995) attempt to find the time delay in the filtered, high frequency portion of the brightness record, and the common experience that the width of any cross-correlation plot yet published is of order 100 days. In future reports we expect to test the assumption further by autocorrelating the wavelet fits to the A and B quasar images to define the fractional quasar *vs* microlensing amplitude at all time scales.

In order to make wavelet decompositions at all time scales we have linearly interpolated the brightness record and then applied corrections for incomplete sampling. In a future report we expect to check these corrections by investigating subsamples of the data with nearly complete sampling. We will also expand our analysis to longer duration wavelets, by analyzing the total 18-year data record rather than the 4-year subsample studied here. We believe that our wavelet fits and missing data corrections are correct to within a factor of two, and this will already allow significant comparisons to microlensing models (which do not yet exist for this system).

Subject to these uncertainties, we report the following conclusions:

1. The mean wavelet amplitude at all time scales is zero, meaning that there are as many negative as positive wavelets.
2. The fitted wavelet amplitudes are equal in the A and B images, except that for the longest fitted wavelets of 64 day duration the B image may have larger amplitude brightness fluctuations.
3. Independently of the family of wavelet fitted or the statistical measure of wavelet



amplitude, the amplitudes seems to increase as a linear function of wavelet duration, with mean absolute deviation a factor of approximately 10 greater for 64-day wavelets than for 2-day ones. A white noise process causing the brightness fluctuations would produce equal mean coefficient amplitudes at all scales, and we conclude that the rapid brightness fluctuations observed in the A and B quasar images are not dominated by observational noise.

## **6. Acknowledgements**

I wish to thank Dr Eric Kolaczyk for helpful remarks about applications of wavelets.

## REFERENCES

- Corrigan, R. T. et al 1991 A.J., 102, 34
- Foufoula-Georgiou, E. & Kumar, P. 1994, Wavelets in Geophysics [New York: Academic Press]
- Haarsma, D., Hewitt, J., Lehar, J., & Burke, B. 1997, ApJ, 479, 102
- Gibson, C., and Schild, R. 1999, A.&A. submitted
- Goicoechea, L., Oscoz, A., Mediavilla, J., & Serra-Ricart, M. 1998 ApJ, 492, 74
- Hjorth, J., Villemoes, L.F., Teuber, J., & Florentin-Nielsen, R. 1992, A.&A. 255, L20
- Kundic, T., Turner, E., Colley, W., Gott III, R., Rhoads, J., Wang, Y., Bergeron, L., Gloria, K., Long, D., Malhotra, S., & Wambsganss, J. ApJ, 482, 75
- Mallat, S. 1989 IEEE Transactions on Pattern Analysis and Machine Intelligence, 11, 674
- Oscoz, A., Mediavilla, E., Goicoechea L., Serra-ricart, M., & Buitrago, J. ApJ, 479, L89
- Pelt, J., Kayser, R., Refsdal, S., & Schramm, T. A. 1996, A&A. 305, 97
- Pelt, J., Schild, R., refsdal, S., Stabell, R., 1998, A.&A. 336, 829
- Scargle, J. 1997 in Applications of Time Series Analysis in Astronomy and Meteorology, ed. T. Subba Rao, M. Priestly, and O. Lessi Chapman and Hall: New York, p. 226
- Schild, R. 1990 AJ, 100, 1771
- Schild, R. 1996 ApJ, 464, 125
- Schild, R. & Cholfin, B. 1986 ApJ, 300, 209
- Schild, R. and Thomson, D. J. 1997 AJ, 113, 130

Slezak, E., Bijaoui, A., and Mars, G. 1990 *A.&A.* 227, 301

Thomson, D.J. & Schild, R. 1997 in *Applications of Time Series Analysis in Astronomy and Meteorology*, ed T. Subba Rao, M. Priestly, and O. Lessi [Chapman and Hall:New York] p187

## FIGURE CAPTIONS

Figure 1a. Wavelet properties for the Coiflet2 (coif2) wavelet. The wavelet shape, called the wavelet function  $\psi$ , is shown in the upper right panel, and the upper left panel shows the associated scaling function  $\phi$ .

Figure 1b. Wavelet properties for the Daubechies 2 (Db2) wavelet, as described in Fig 1a.

Figure 1c. Wavelet properties for the Daubechies 3 (Db3) wavelet, as described in Fig 1a.

Figure 2. A full wavelet decomposition for the 4-year data subset of the A (northern) quasar image with a second order Coiflet (Coif2) analyzing wavelet. The signal analyzed in the upper left panel is labeled  $s$ . The lower right panel labeled d1 shows the details of fitting the wavelets with a 2-day width to the signal, and the lower left panel labeled a1 shows an approximation to the signal with the details of d1 removed. So adding coif 2 wavelets of amplitude given in d1 to the residual signal a1 produces an exact reconstruction of the signal  $s$ . Similarly panel d2 shows the details of a wavelet fit to a1, and the residual signal with the d2 wavelets removed is seen in panel a2. An exact reconstruction of signal  $s$  is obtained by adding to signal a2 a pattern of coif 2 wavelets having 4 day duration and amplitudes d2, together with a pattern of 2-day duration wavelets having amplitudes given in d1. Similarly, panels d3...d6 show the patterns of wavelets which when fitted to the signal give approximations a3...a6. The original signal is thus decomposed into the 6 signals d1...d6 by which coif2 wavelets of duration 2...64 days are multiplied and added to residual signal a6 for an optimum wavelet representation of the original signal. The power of this approach is that the six detail signals d1...d6 now provide the basis for detailed estimation of numerous properties of the original signal, such as the power in negative *vs* positive wavelets and the amount of wavelet power as a function of wavelet duration. Such

properties obviously relate to the physical process producing the brightness fluctuations, and our purpose is to provide a quantitative means of comparing observations to model simulations.

Figure 3. A Coif2 full wavelet decomposition of the 4-year data subset of the B (southern) quasar image.

Figure 4. A wavelet analysis of a quiet subset of the A brightness record. The bottom panels d1 and d2 show the Coif2 wavelets of 2- and 4-day width fitted to the A quasar image signal  $s$ .

Figure 5. The mean absolute deviation measure of wavelet amplitude as a function of wavelet duration for the A and B quasar images, and for the three analyzing wavelets as identified. Thus the curve marked B-Db3 shows the wavelet amplitude for the B quasar image with the Daubechies 3 analyzing wavelet.

Figure 6. The corrected mean absolute deviation measure of wavelet amplitude for the Coif2 analyzing wavelet applied to the A and B quasar images, with corrections for missing data applied as noted in the text.

Figure 7. The standard deviation measure of wavelet amplitude as a function of wavelet duration, with the several curves identified as in Fig. 5

Figure 8. The corrected standard deviation measure of wavelet amplitude for the Coif2 analyzing wavelet applied to the A and B quasar images, with corrections for missing data and interpolation applied as noted in the text.

Table 1. Mean values

Image	Wavelet	d1	d2	d3	d4	d5	d6
A	Coif2	-.00702	-.02151	-.00141	.00018	.00197	.01187
...	Db2	-.01080	.04512	-.00186	.04895	-.00869	-.00011
...	Db3	-.00771	-.00013	.00026	.00052	-.00128	-.00978
...	mean	-.00851	.00783	-.00100	.01655	-.00267	.00066
...	rms	.00201	.03402	.00112	.02806	.00546	.01085
B	Coif2	-.01238	-.04371	-.00139	-.00369	.00044	.00437
...	Db2	-.02449	.00037	-.00148	-.00347	-.00209	-.01903
...	Db3	-.00674	-.00036	-.03605	.00028	-.00050	-.02353
...	mean	-.01454	-.01457	-.01297	-.00229	-.00072	-.01273
...	rms	.00907	.02524	.01999	.00223	.00128	.01498

Table 2. Mean absolute deviation

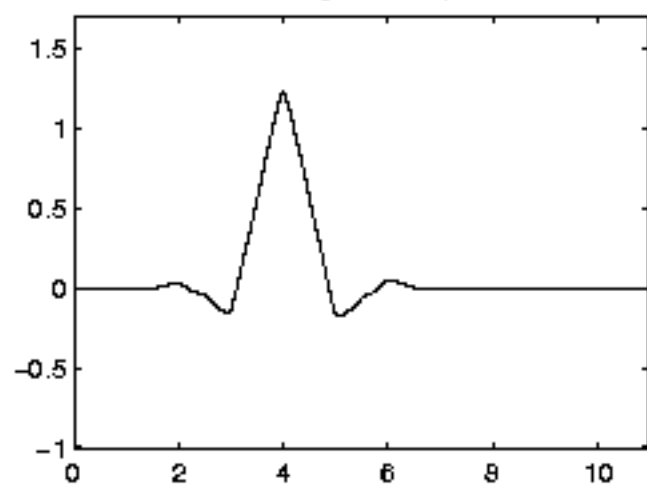
Image	Wavelet	d1	d2	d3	d4	d5	d6
A	Coif2	.002284	.005104	.01046	.01732	.03142	.05854
...	Db2	.002492	.005236	.01086	.01698	.03585	.05583
...	Db3	.002434	.005345	.00916	.01811	.03566	.06099
...	mean	.00240	.00523	.01016	.01747	.03331	.05845
...	std	.00011	.00012	.00089	.00058	.00216	.00258
...	corr	2.88	1.736	1.536	1.377	1.226	1.165
...	crted	.00691	.00908	.01561	.02406	.04058	.06804
B	Coif2	.002126	.004785	.01059	.01703	.02495	.06409
...	Db2	.002254	.005669	.01072	.01671	.03822	.07733
...	Db3	.002258	.005077	.01001	.01792	.03057	.09169
...	mean	.00221	.00518	.01044	.01722	.03125	.0776
...	std	.00008	.00045	.00038	.00063	.00666	.01380
...	corr	2.88	1.736	1.536	1.377	1.226	1.165
...	crted	.00636	.00899	.01604	.02371	.03831	.09051

Table 3. Std. deviation measure of wavelet amplitudes

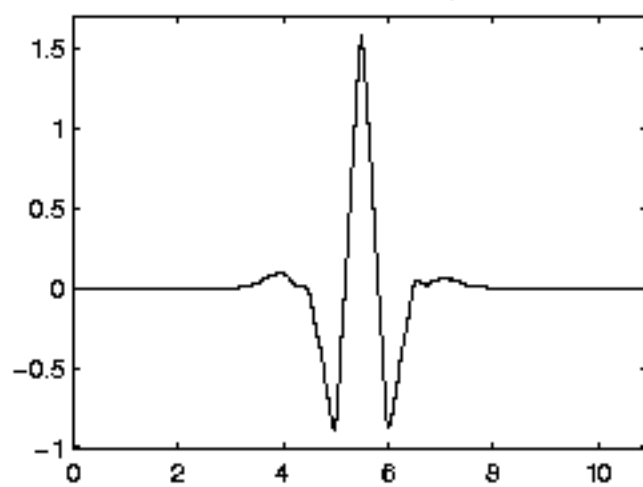
Image	Wavelet	d1	d2	d3	d4	d5	d6
A	Coif2	.005315	.008599	.01622	.02378	.04586	.08241
...	Db2	.005421	.009639	.01722	.02524	.04837	.07441
...	Db3	.005288	.009154	.01360	.02706	.04955	.08056
...	mean	.00534	.00913	.01567	.02536	.04793	.07913
...	std	.00007	.00052	.00186	.00164	.00188	.00419
...	corr	2.1294	1.2416	1.1346	1.0687	1.0252	1.0135
...	crted	.01137	.01134	.01778	.02710	.04914	.08020
B	Coif2	.00479	.00784	.01604	.02457	.03566	.09171
...	Db2	.00482	.009510	.01594	.02235	.05422	.1033
...	Db3	.00453	.008360	.01512	.02727	.04060	.12322
...	mean	.00472	.00857	.01570	.02473	.04349	.10607
...	std	.00016	.00085	.00050	.00246	.00961	.01593
...	corr	2.1294	1.2416	1.1346	1.0687	1.0252	1.0135
...	crted	.01005	.01064	.01781	.02643	.04459	.10750



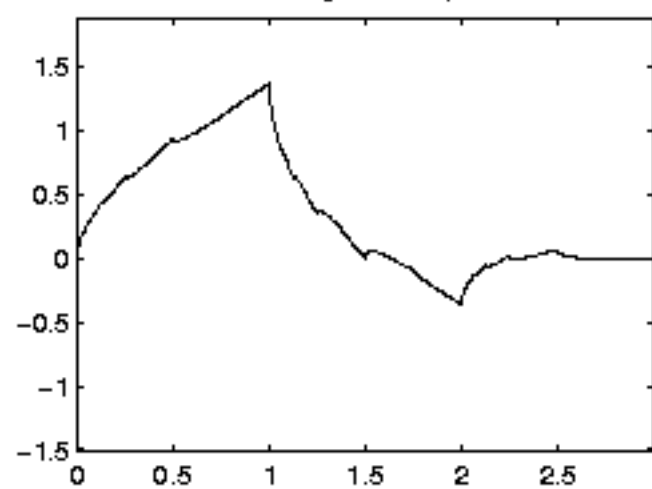
Scaling function  $\phi$



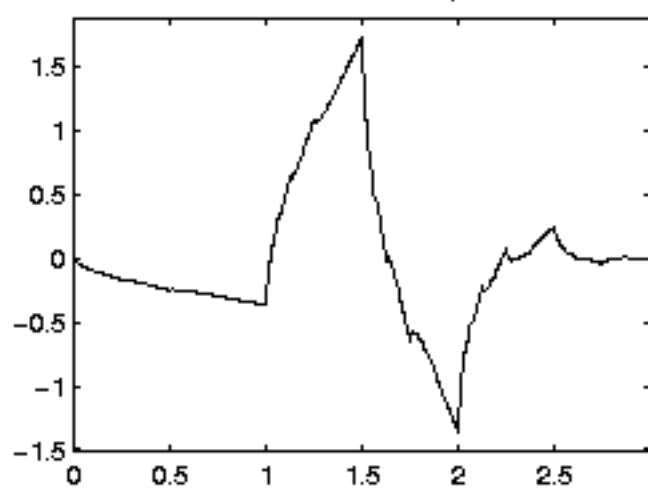
Wavelet function  $\psi$



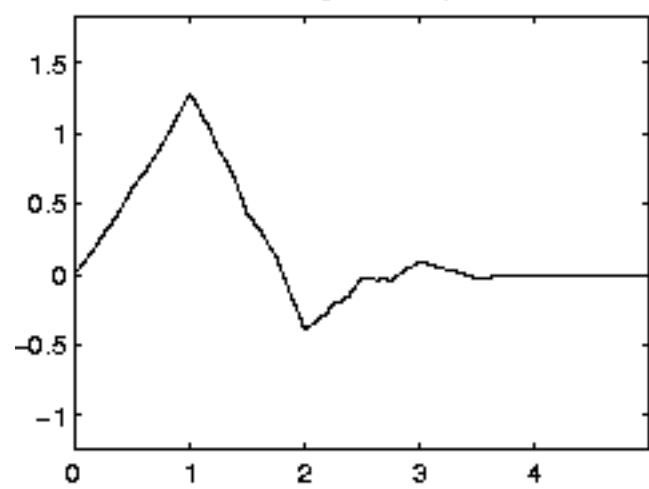
Scaling function  $\phi$



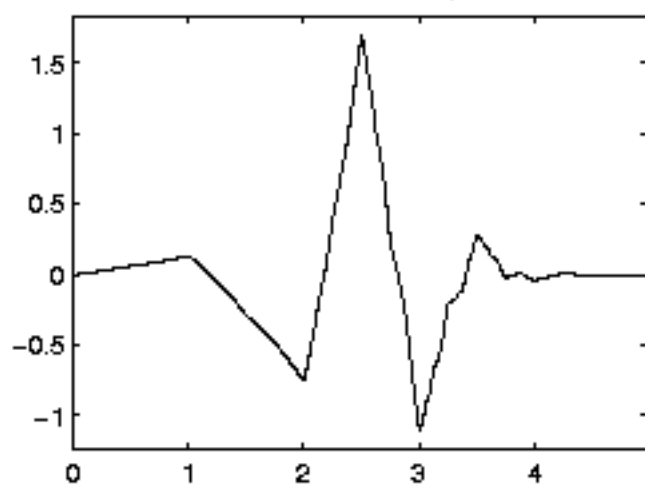
Wavelet function  $\psi$

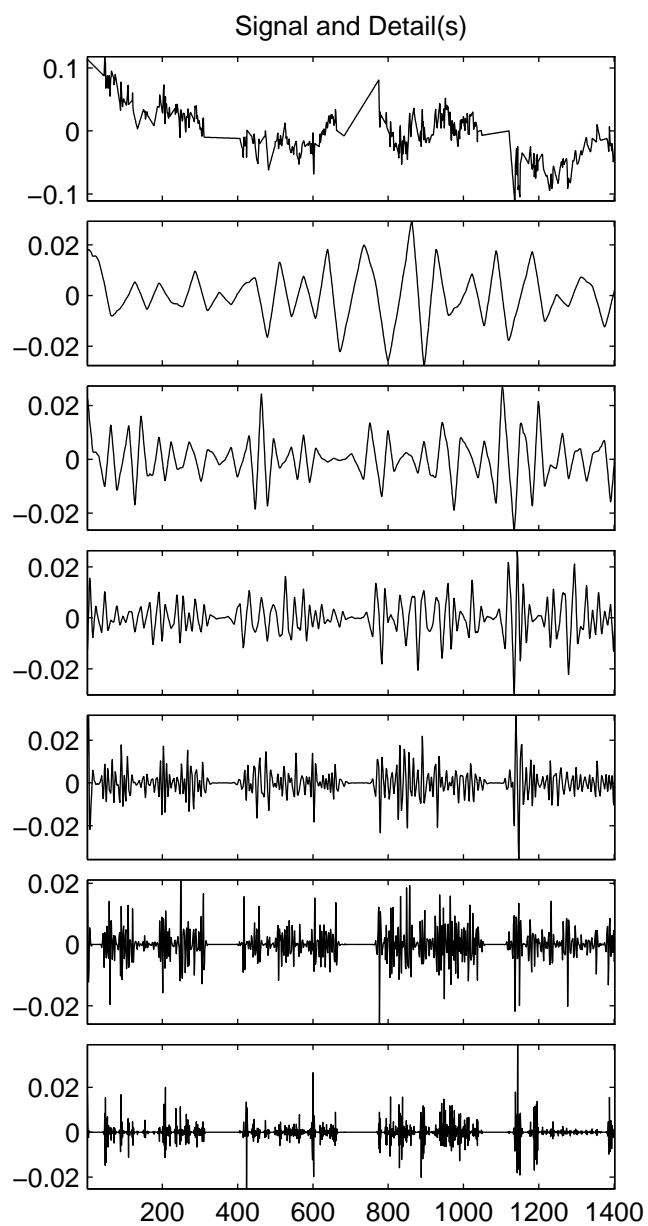
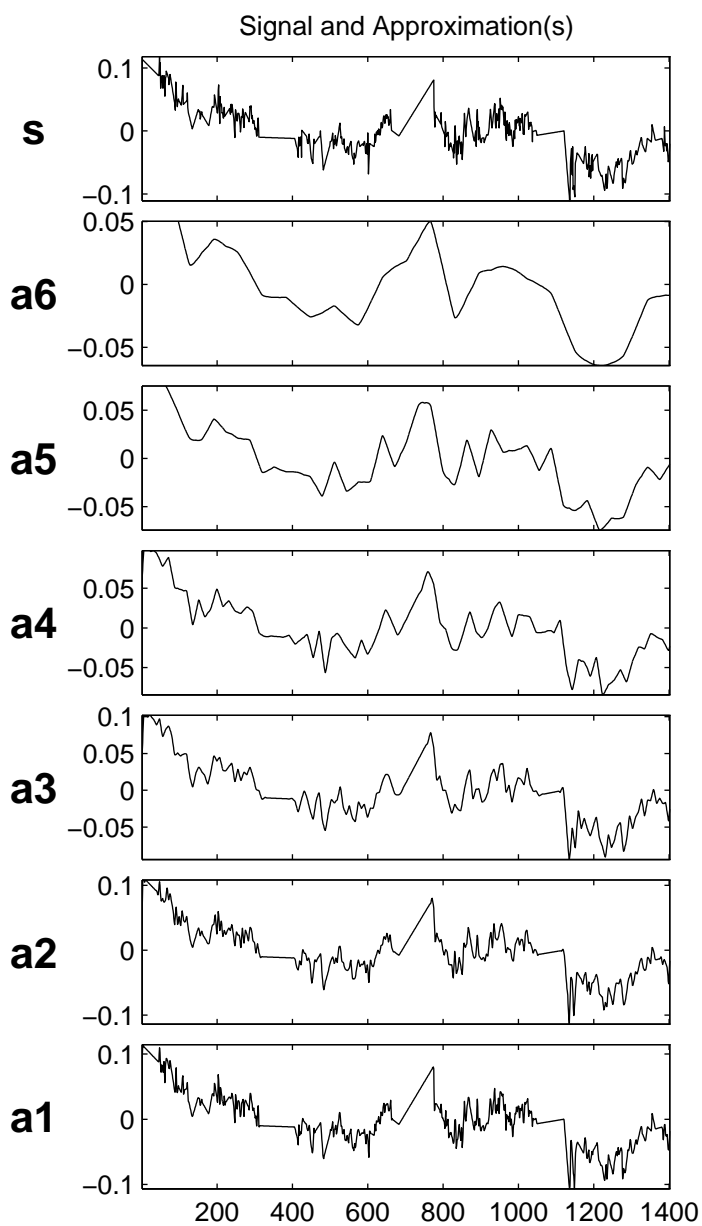


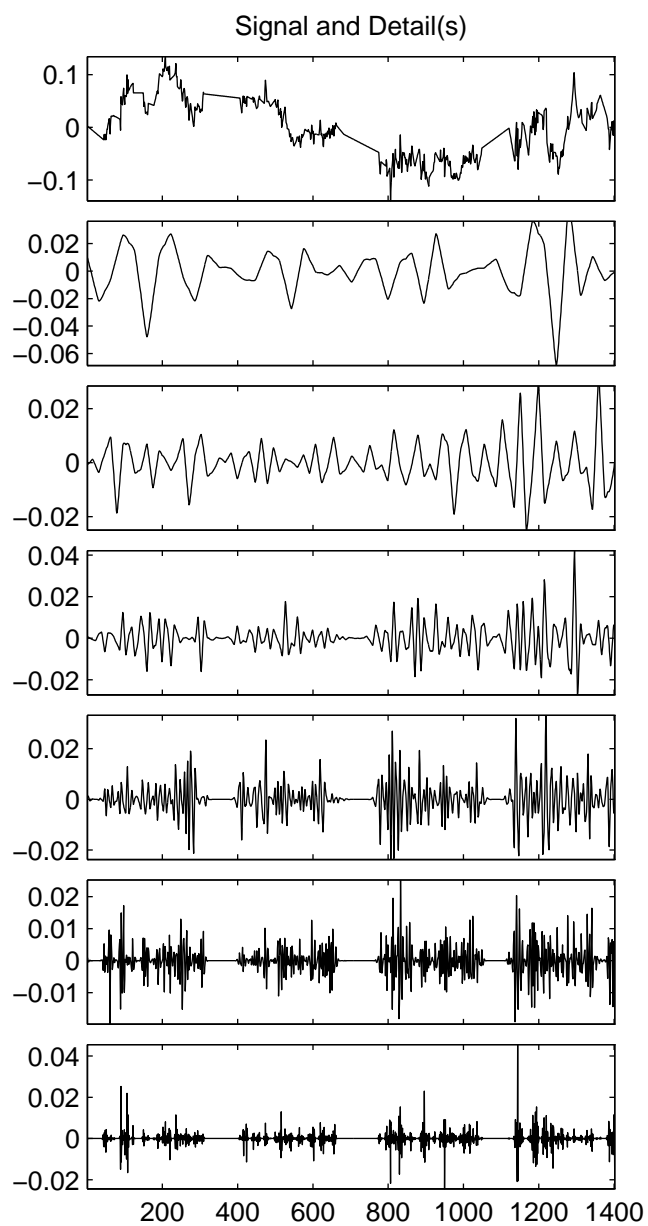
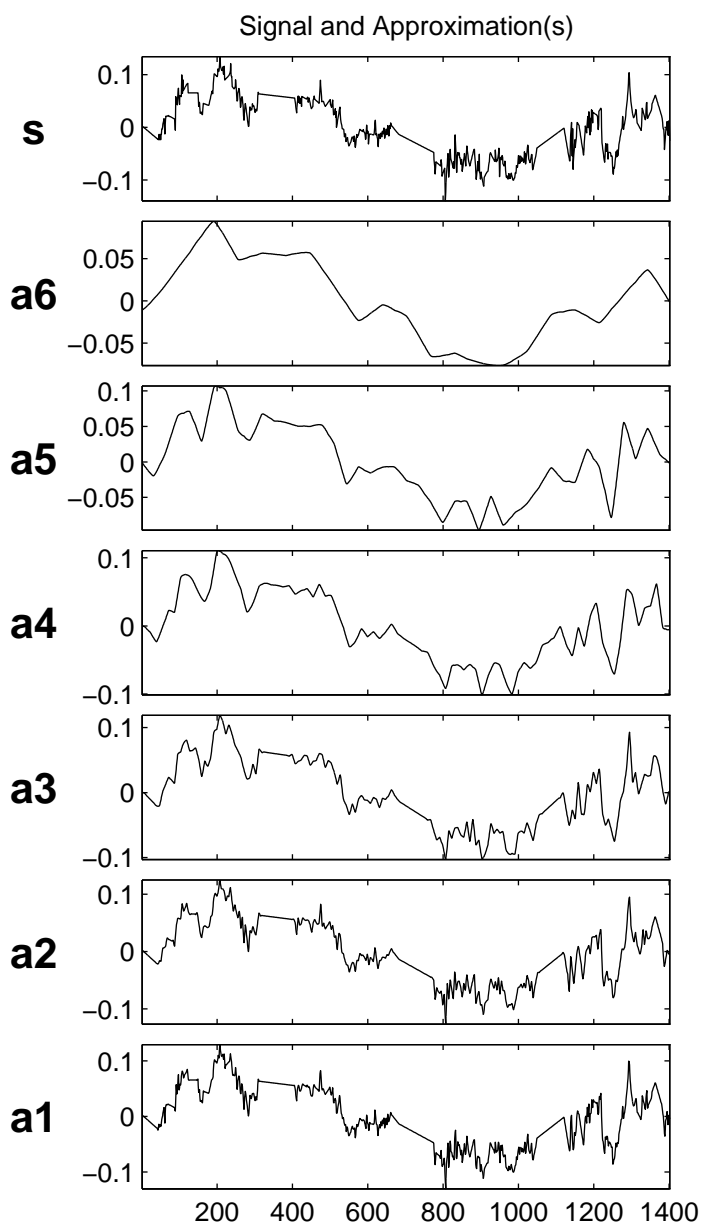
Scaling function  $\phi$



Wavelet function  $\psi$







Decomposition at level 2 :  $s = a2 + d2 + d1$  .

